Physics and Imaging in Radiation Oncology 23 (2022) 44–47

Contents lists available at ScienceDirect

Physics and Imaging in Radiation Oncology

journal homepage: www.sciencedirect.com/journal/physics-and-imaging-in-radiation-oncology

Technical Note

Comparison of compressed sensing and controlled aliasing in parallel imaging acceleration for 3D magnetic resonance imaging for radiotherapy preparation

Frederik Crop [a,*], Ophélie Guillaud [b], Mariem Ben Haj Amor [b], Alexandre Gaignierre [b], Carole Barre [c], Cindy Fayard [b], Benjamin Vandendorpe [c], Kaoutar Lodyga [c], Raphaëlle Mouttet-Audouard [c], Xavier Mirabel [b]

[a] Medical Physics, Centre Oscar Lambret, Lille, 3 Rue Frédéric Combemale, 59000 Lille, France
[b] Radiology, Centre Oscar Lambret, Lille, 3 Rue Frédéric Combemale, 59000 Lille, France
[c] Academic Department of Radiotherapy, Centre Oscar Lambret, Lille, 3 Rue Frédéric Combemale, 59000 Lille, France

ARTICLE INFO

Keywords:
Magnetic resonance imaging
Signal-to-noise ratio
Compressed sensing
Radiotherapy
CAIPIRINHA
3D SPACE

ABSTRACT

Magnetic resonance imaging (MRI) for radiotherapy is often based on 3D acquisitions, but suffers from low signal-to-noise ratio due to immobilization device and flexible coil use. The aim of this study was to investigate if Compressed Sensing (CS) improves image quality for 3D Turbo Spin Echo acquisitions compared with Controlled Aliasing k-space-based parallel imaging in equivalent acquisition time for intracranial T1, T2-Fluid-Attenuated Inversion Recovery (FLAIR) and pelvic T2 imaging. Qualitative ratings suffered from large inter-rater variability. CS-T1 brain MRI was superior numerically and qualitatively. CS-T2-FLAIR brain MRI was numerically superior, but rater equivalent. CS-T2 pelvic MRI was equivalent without gain.

1. Introduction

Magnetic Resonance Imaging (MRI) for radiotherapy (RT) suffers from an inherently low signal-to-noise ratio (SNR) due to the utilization of immobilization devices, inability to use a dedicated Head and Neck coil, but also flat couch top or coil arches [1]. This results in lower image quality for MRI for RT and is often compensated by lower resolution or additional scan time. But adding averages results only in square root SNR gain and high 3D resolution and bandwidth is required for improved Computed Tomography (CT)-MRI fusion and contouring [1,2]. A promising approach of this problem is the use of Super Resolution (SR) techniques [3–6], but they were not clinically available for 3D imaging at the time of writing this study. Instead of searching for an equivalent image quality in a shorter time as often studied in diagnostic imaging [7–11], our study focused on searching for an improved image quality (resolution/contrast) in an equivalent time using Compressed Sensing (CS) [8,9,12–14] instead of CAIPIRINHA (Controlled Aliasing in Parallel Imaging Results in Higher Acceleration) acceleration [15]. A first step was to iteratively obtain clinically practical acceleration and regularization values as neither the vendor or literature could provide guidance for 3D imaging in an RT setting at the time of the study [9,10]. This was followed by the presented phantom and patient study to quantify differences.

2. Materials and methods

2.1. Sequences and patient setup

The SPACE (Sampling Perfection with Application optimized Contrasts using different flip angle Evolution) sequence is a 3D Turbo Spin Echo (TSE) technique using a variable flip angle during the echo train [16]. CAIPIRINHA acceleration is a k-space-based parallel imaging technique which uses both undersampled k-space data and calibration lines acquired in the center of the k-space. A fit is performed between the data from all coil elements and calibration lines and is then used to fill in the missing k-space data for the individual coil images [17,18], but can lead to unexpected artefacts [8,19]. CS applies random k-space undersampling in phase encoding directions in order to measure incoherently in k-space: as of such, artifacts become noise-like in the transformed domain. CS is best applicable in images which are sparse in a transform

* Corresponding author at: Medical Physics, Centre Oscar Lambret, Lille, France.
E-mail address: F-Crop@o-lambret.fr (F. Crop).

https://doi.org/10.1016/j.phro.2022.06.008
Received 11 January 2022; Received in revised form 9 June 2022; Accepted 20 June 2022
Available online 23 June 2022

domain, such as the wavelet domain or temporal fourier domain [9,12–14,20]. Regularization factors which regulate data consistency, are also application specific. The CS implementation was based on a Sensitivity Encoding optimization using a fast iterative shrinkage-thresholding and a Haar wavelet transform for spatial regularization [21,22]. The undersampling pattern was based on a Poisson-disc pattern and a spiral trajectory was applied.

CS acceleration can result in different artifacts [8]: wax layer, streaky-linear, (types A, B, and C), and starry sky artifacts. Higher "conventional" acceleration can result in the loss of high-contrast details, whereas with CS, this tradeoff is different. Instead of resolution, CS can lead for example to loss of low-contrast details. In vivo iterations were performed (resolution, CS and turbo acceleration factors, denoising factor, repetition time…) until the qualitative best result was obtained with respect to artifacts or the appearance of "blocky" images for CS images. After multiple parameter iterations in vivo and on phantom (SNR), acquisitions with optimal values were applied in vivo and on phantom for this study. The goal was to "use" improved CS SNR to improve contrast but also resolution/bandwidth whilst the acquisition time was maintained as a constant. For T1, contrast was improved through repetition time (TR) reduction whereas for T2-Fluid-Attenuated Inversion Recovery (FLAIR) Echo Train Length (ETL) reduction was applied.

CS acquisitions applied higher acquired resolutions, but not always the reconstructed resolution: when the reconstructed voxel is smaller than the acquired voxel, streaking artifacts may occur (type A artifact for CS [8]). Immobilization devices, sequence parameters and flexible coils are detailed in the Supplementary Table 1. MRI scans were performed on a 1.5 T Sola MRI scanner (Siemens, Erlangen, Germany).

2.2. Phantom acquisitions and SNR evaluation

Relative SNR of CS-to-CAIPI was evaluated on a Magphan 170 phantom (the phantom laboratory, NY, USA) filled with $CuSO_4$ solution by applying the NEMA difference method [23]. Two acquisitions were performed for each acceleration technique in order to create both a mean and a subtracted/background image. μ corresponds to the mean signal intensity in the region-of-interest (ROI) of the mean image whereas σ_{diff} corresponds to the noise in the ROI of the difference image. The SNR was then evaluated using:

$$SNR_{NEMA1,diff} = \sqrt{2}\,\frac{\mu}{\sigma_{diff}}$$

in seven different ROIs (center, left, right, superior, inferior, anterior, and posterior), in order to reflect the g factor [17,24]. Owing to parallel imaging acceleration, the noise can be located in specific regions. For example, in brain studies with k-space based acceleration, noise can be concentrated in the posterior fossa especially when using neck immobilization support. For the T2-FLAIR sequence, the SNR in the inserts was also evaluated as otherwise, mainly noise was evaluated due to the fluid attenuation. The SNR evaluation in a CS acquisition was also influenced by the denoising algorithm. Therefore, the SNR was also evaluated by reconstruction of the images with a denoising factor of 1 (regularization $\lambda = 0.00001*DEN^2$). Accuracy of SNR_{NEMA} was not evaluated in detail for all sequence types, but the mean relative SNR (CS)/SNR(CAIPI) for each ROI of three reproductions on different days was reported with appropriate uncertainty intervals from the literature [25].

2.3. Patient acquisitions

During a three-month-period, a CS and CAIPIRINHA-based sequence was acquired for patients. This concerned for intracranial T1 images ten patients representing 17 metastasis. For T2-FLAIR this concerned eight patients representing three gliomas and seven metastasis. Finally, T2 pelvic MRI was acquired for seven patients. T2-FLAIR aids in contouring as it can be used for evaluation of edema, infiltration, leaky blood–brain barrier and has higher (lepto)meningeal metastasis sensitivity [26,27]. Contrast enhancement in the intracranial images was influenced by the timing after contrast agent administration. Thus, the timing of the CAIPIRINHA and CS sequences was randomized for each patient, at least 4 min after contrast agent injection. Patient consent was obtained for anonymous use of the data.

2.4. Quantitative lesion contrast evaluation

Contrast Ratios (CR) were evaluated between the mean signal intensity (SI) of the enhanced lesion and the brainstem:

$$CR = \frac{SI_{lesion} - SI_{brainstem}}{SI_{brainstem}}$$

The CR for each acceleration technique was compared using Bland-Altman plots [28]. A paired one-sided *t*-test was also applied on a $p = 0.05$ level using the R project [29]. A one-sided *t*-test could be justified as improved contrast due to TR reduction for T1 and ETL reduction for T2-FLAIR could be expected. The contrast-to-noise ratio (CNR) was not evaluated: CS denoising results in an artificial lower noise, thus resulting in a higher CNR. Repeated acquisitions for noise evaluations were ethically unjustified for patients.

2.5. Qualitative rater evaluation

Three expert radiologists and four expert radiation oncologists evaluated eight T1, seven T2-FLAIR and seven T2 prostate MRIs of both acceleration techniques in the PACS, (Telemis, Louvain-La-Neuve, Belgium) in an anonymized and randomized alternative choice test that tested the preference for image A vs. B or equivalent. No information on the differences between the images was provided before. Preference for CS scored 1, for CAIPIRINHA-1 or 0 for equivalent. The results were analyzed using the R project [29] for significance by a Wilcoxon signed rank test, and agreement between raters was evaluated by a pairwise Cohen Kappa test. A contouring study was not performed as contouring is based on a set of images, but also the inter/intra rater variability was very large [30].

3. Results

Fig. 1 shows more uniform SNR throughout the phantom with CS, especially for the otherwise noisy posterior fossa region, combined with smaller voxel size and contrast improvements (TR/ETL) for both CS-T1 and CS-T2-FLAIR. Pelvic CS-T2 could not improve considerably SNR and as of such voxel size or contrast were not improved considerably.

An increase in CRs for patient T1 and T2-FLAIR images can be observed in the Bland-Altman plots of Fig. 2a and b. The CRs were statistically significant increased on a one sided paired *t*-test: 0.1 (95% CI $[0.04;\infty]$, $p = 0.004$) for T1 and 0.1 (95% CI $[0.01;\infty]$, $p = 0.03$) for T2-FLAIR. 95% CIs for two sided *t*-test, corresponding to the 95% Bland-Altman confidence interval of the mean difference were [0.03;0.16] and [-0.006;0.2]. This corresponded to relative signal gains (lesion-to-brainstem) of 7% and 4% for T1 and T2-FLAIR respectively.

Mean qualitative ratings, shown in Fig. 2c with examples in Supplementary Figs. 1–3, in the interval [1,-1] with positive values favoring CS were: T1 = 0.5 ($p < 0.05$), T2-FLAIR = -0.2 ($p > 0.05$), and T2 prostate = 0 ($p > 0.05$). Concordance between raters was, however, low as pairwise Cohen kappa results were respectively < 0.31, < 0.33 and < 0.4 for the three sequences. No two raters had good interrater reliability.

4. Discussion

This study compared two acceleration techniques for radiotherapy MRI, using flexible coils and immobilization devices. CS was favored for

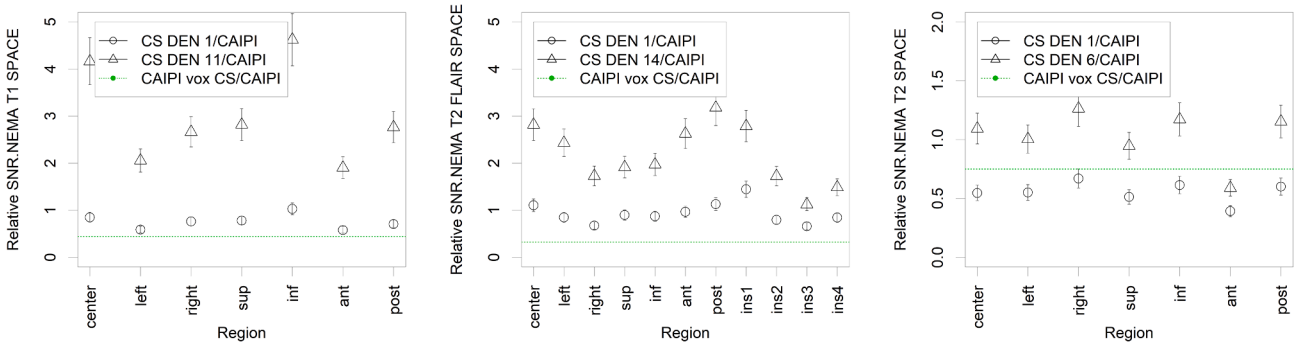

Fig. 1. Relative SNR, compared to CAIPIRINHA acquisition, for the different regions in magphan phantom. The dashed green line represents the theoretical SNR for the CAIPIRINHA acceleration if the voxel size and bandwidth were equivalent to the CS acquisition. Results are the mean of three reproductions and uncertainty bars represent 1 σ.

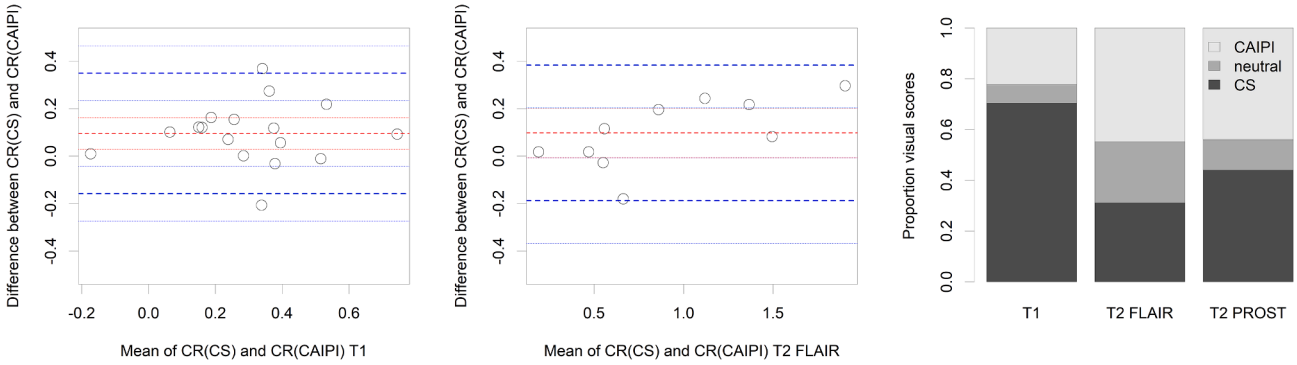

Fig. 2. Bland-Altman plots of Contrast Ratios for both CS and CAIPIRINHA accelerated sequences, post-contrast agent (T1: a, T2: b). Fig. 2c represents the visual scoring of expert readers.

intracranial T1 and T2-FLAIR, but not for pelvic T2. CS-T1 and CS-T2-FLAIR obtained more homogeneous SNR throughout the phantom compared to CAIPIRINHA acceleration, resulting in a better homogeneous control of noise. However, this was not the case for pelvic T2. The gain in SNR not only allowed a higher resolution but also better contrast for T1 images by lowering the TR. This was confirmed in the overall contrast gain for almost all lesions, even when the CS sequence being performed first. Comparison with literature was difficult, as most studies were in a diagnostic setting, focus on time gains or 2D-CS, and compare to other acceleration techniques. The CS-T1 factor of 4.4 was higher than the value obtained by [31] most likely due to the dedicated Head-and-Neck coil use.

The CS-T2-FLAIR sequence delivered a slightly better contrast most likely due to ETL lowering, but this was only borderline statistically significant on a one sided test. There was also a bias in sequencing, i.e., the CAIPIRINHA sequence was performed more often first. T2-FLAIR ratings showed interrater variability: one expert rater specifically preferred the texture of the CAIPIRINHA acceleration over the CS texture. This resulted in a general equivalent note, but offered a higher 3D resolution with CS which was perhaps not necessary. In practice, following these results, an intermediate was taken using an inbetween 3D resolution, TR at 8000 ms, and reduction of 1 min acquisition time. Other studies obtained both higher [8] or lower [32] CS-T2-FLAIR factors.

T2 pelvic results resulted in a mean 0 score. It should be noted that blood vessels appeared better with CS, but detailed bone structures were visualized better with CAIPIRINHA acceleration. Raters reported that visual hypo intense contrast of lesions was often better with CS acceleration. However, visual inferior anatomical information made them rate CAIPIRINHA as often as superior. No significant gain in SNR and thus possible resolution/contrast gain was possible. This indicates that other techniques, such as SR techniques [3] or direct denoising techniques could be better approaches. A recent study [33] applied CS to radiotherapy MRI for prostate 3D-T2. Slightly higher CS factors of 7.3 were used, but they compared to 2D imaging. Their study focused further on time reduction, 2D imaging and was compared to Sensitivity Encoding. The current study used CAIPIRINHA-k-space based acceleration as baseline which could possibly perform better.

A study limit is that rating can show variability depending on the software and screens used. The number of the studied images was limited, which might lead to limited statistical power. However the discordance between the seven raters was found to be high, which is expected to persist: the CS texture was different which leads to rater differences. This confirms in more detail the results of another CS study with two raters [33]. Radiomics or conversion to pseudo-CT images [34,35] from CS accelerated MRI will also require quality control as the texture is different.

In conclusion, CS acceleration was evaluated as superior both numerically and by visual rating for 3D intracranial T1. Brain T2-FLAIR MRI for RT was numerically superior with CS, but rated visually as equal to CAIPIRINHA. Pelvic T2 was evaluated as equivalent. Finally, visual rating of CS versus CAIPIRINHA acceleration suffered from large inter-rater variability.

Declaration of Competing Interest

The authors declare that they have no known competing financial interests or personal relationships that could have appeared to influence the work reported in this paper.

Acknowledgement

We wish to thank Editage for English language corrections. We wish to thank the GIP Cancéropôle Nord-Ouest for their support.

Appendix A. Supplementary data

Supplementary data to this article can be found online at https://doi.org/10.1016/j.phro.2022.06.008.

References

[1] Glide-Hurst CK, Paulson ES, McGee K, Tyagi N, Hu Y, Balter J, et al. Task group 284 report: magnetic resonance imaging simulation in radiotherapy: considerations for clinical implementation, optimization, and quality assurance. Med Phys 2021;48. https://doi.org/10.1002/mp.14695. e636-70.
[2] Brock KK, Mutic S, McNutt TR, Li H, Kessler ML. Use of image registration and fusion algorithms and techniques in radiotherapy: Report of the AAPM Radiation Therapy Committee Task Group No. 132. Med Phys 2017;44:e43–76. doi:10.1002/mp.12256.
[3] Küstner T, Munoz C, Psenicny A, Bustin A, Fuin N, Qi H, et al. Deep-learning based super-resolution for 3D isotropic coronary MR angiography in less than a minute. Magn Reson Med 2021;86:2837–52. https://doi.org/10.1002/MRM.28911.
[4] Shi J, Liu Q, Wang C, Zhang Q, Ying S, Xu H. Super-resolution reconstruction of MR image with a novel residual learning network algorithm. Phys Med Biol 2018;63. doi:10.1088/1361-6560/AAB9E9.
[5] Pham CH, Tor-Díez C, Meunier H, Bednarek N, Fablet R, Passat N, et al. Multiscale brain MRI super-resolution using deep 3D convolutional networks. Comput Med Imaging Graph 2019;77. doi:10.1016/J.COMPMEDIMAG.2019.101647.
[6] Chen Y, Christodoulou AG, Zhou Z, Shi F, Xie Y, Li D. MRI Super-Resolution with GAN and 3D Multi-Level DenseNet: Smaller, Faster, and Better. [Preprint] 2020. doi:10.48550/arxiv.2003.01217.
[7] Toledano-Massiah S, Sayadi A, De Boer R, Gelderblom J, Mahdjoub R, Gerber S, et al. Accuracy of the Compressed Sensing Accelerated 3D-FLAIR Sequence for the Detection of MS Plaques at 3T. AJNR Am J Neuroradiol 2018;39:454–8. https://doi.org/10.3174/AJNR.A5517.
[8] Sartoretti T, Reischauer C, Sartoretti E, Binkert C, Najafi A, Sartoretti-Schefer S. Common artefacts encountered on images acquired with combined compressed sensing and SENSE. Insights Imag 2018;9:1107–15. https://doi.org/10.1007/s13244-018-0668-4.
[9] Jaspan ON, Fleysher R, Lipton ML. Compressed sensing MRI: a review of the clinical literature. Br J Radiol 2015;88:20150487. https://doi.org/10.1259/bjr.20150487.
[10] She H, Chen RR, Liang D, Dibella EVR, Ying L. Sparse BLIP: BLind Iterative Parallel imaging reconstruction using compressed sensing. Magn Reson Med 2014;71:645–60. https://doi.org/10.1002/MRM.24716.
[11] H. Blaise T. Remen K. Ambarki E. Weiland B. Kuehn X. Orry et al. Comparison of respiratory-triggered 3D MR cholangiopancreatography and breath-hold compressed-sensing 3D MR cholangiopancreatography at 1.5 T and 3 T and impact of individual factors on image quality Eur J Radiol 2021;142:109873. 10.1016/J.EJRAD.2021.109873.
[12] Fornasier M, Rauhut H. Compressive Sensing. New York: Springer; 2011. doi:10.1007/978-0-387-92920-0_6.
[13] Geethanath S, Reddy R, Konar AS, Imam S, Sundaresan R, Ramesh Babu DR, et al. Compressed sensing MRI: a review. Crit Rev Biomed Eng 2013;41:183–204. https://doi.org/10.1615/CritRevBiomedEng.2014008058.
[14] Lustig M, Donoho DL, Santos JM, Pauly JM. Compressed sensing MRI: A look at how CS can improve on current imaging techniques. IEEE Signal Process Mag 2008;25:72–82. https://doi.org/10.1109/MSP.2007.914728.
[15] Breuer FA, Blaimer M, Heidemann RM, Mueller MF, Griswold MA, Jakob PM. Controlled aliasing in parallel imaging results in higher acceleration (CAIPIRINHA) for multi-slice imaging. Magn Reson Med 2005;53:684–91. https://doi.org/10.1002/mrm.20401.
[16] Mugler JP. Optimized three-dimensional fast-spin-echo MRI. J Magn Reson Imaging 2014;39:745–67. https://doi.org/10.1002/jmri.24542.
[17] Larkman DJ, Nunes RG. Parallel magnetic resonance imaging. Phys Med Biol 2007;52:R15–55. https://doi.org/10.1088/0031-9155/52/7/R01.
[18] Breuer FA, Blaimer M, Mueller MF, Seiberlich N, Heidemann RM, Griswold MA, et al. Controlled aliasing in volumetric parallel imaging (2D CAIPIRINHA). Magn Reson Med 2006;55:549–56. https://doi.org/10.1002/mrm.20787.
[19] Crop F, Mouttet-Audouard R, Mirabel X, Ceugnart L, Lacornerie T. Unexpected external markers artifact in 3D k-space based parallel imaging turbo spin-echo magnetic resonance imaging. Phys Med 2021;90:150–7. https://doi.org/10.1016/j.ejmp.2021.10.001.
[20] Lustig M, Donoho D, Pauly JM. Sparse MRI: the application of compressed sensing for rapid MR imaging. Magn Reson Med 2007;58:1182–95. https://doi.org/10.1002/MRM.21391.
[21] Pruessmann KP, Weiger M, Börnert P, Boesiger P. Advances in sensitivity encoding with arbitrary k-space trajectories. Magn Reson Med 2001;46:638–51. https://doi.org/10.1002/MRM.1241.
[22] Liang D, Liu B, Wang J, Ying L. Accelerating SENSE using compressed sensing. Magn Reson Med 2009;62:1574–84. https://doi.org/10.1002/MRM.22161.
[23] Magnetic Resonance Imaging Quality Control Manual, American College of Radiology, Committee on QA in MRI 2015.
[24] Larkman DJ. The g-Factor and Coil Design. Parallel Imaging Clin. MR Appl., Heidelberg, Berlin: Springer Berlin Heidelberg; 2007, p. 37–48. doi:10.1007/978-3-540-68879-2_3.
[25] Dietrich O, Raya JG, Reeder SB, Reiser MF, Schoenberg SO. Measurement of signal-to-noise ratios in MR images: Influence of multichannel coils, parallel imaging, and reconstruction filters. J Magn Reson Imaging 2007;26:375–85. https://doi.org/10.1002/JMRI.20969.
[26] Park YW, Ahn SJ. Comparison of contrast-enhanced T2 FLAIR and 3D T1 black-blood fast spin-echo for detection of leptomeningeal metastases. Investig Magn Reson Imaging 2018;22:86. https://doi.org/10.13104/IMRI.2018.22.2.86.
[27] Jeevanandham B, Kalyanpur T, Gupta P, Cherian M. Comparison of post contrast 3D T1 MPrage, 3D T1 space and 3D T2 FLAIR MR Images in evaluation of meningeal abnormalities at 3T MRI 2017:1–10. doi:10.1259/bjr.20160834.
[28] Martin Bland J, Altman DG. Statistical methods for assessing agreement between two methods of clinical measurement. Lancet 1986;327:307–10. https://doi.org/10.1016/S0140-6736(86)90837-8.
[29] Ripley BD. The R project in statistical computing. MSOR Connect 2001:23–5. https://doi.org/10.11120/MSOR.2001.01010023.
[30] Mazzara GP, Velthuizen RP, Pearlman JL, Greenberg HM, Wagner H. Brain tumor target volume determination for radiation treatment planning through automated MRI segmentation. Int J Radiat Oncol Biol Phys 2004;59:300–12. https://doi.org/10.1016/J.IJROBP.2004.01.026.
[31] Sartoretti T, Sartoretti E, Wyss M, Schwenk Á, van Smoorenburg L, Eichenberger B, et al. Compressed SENSE accelerated 3D T1w black blood turbo spin echo versus 2D T1w turbo spin echo sequence in pituitary magnetic resonance imaging. Eur J Radiol 2019;120. https://doi.org/10.1016/J.EJRAD.2019.108667.
[32] Sharma SD, Fong CL, Tzung BS, Law M, Nayak KS. Clinical image quality assessment of accelerated magnetic resonance neuroimaging using compressed sensing. Invest Radiol 2013;48:638–45. https://doi.org/10.1097/RLI.0B013E31828A012D.
[33] Yu VY, Zakian K, Tyagi N, Zhang M, Romesser PB, Dresner A, et al. Combined compressed sensing and SENSE to enhance radiation therapy magnetic resonance imaging simulation. Adv Radiat Oncol 2022;7:100799. https://doi.org/10.1016/J.ADRO.2021.100799.
[34] Brou Boni KND, Klein J, Vanquin L, Wagner A, Lacornerie T, Pasquier D, et al. MR to CT synthesis with multicenter data in the pelvic area using a conditional generative adversarial network. Phys Med Biol 2020;65:075002. https://doi.org/10.1088/1361-6560/AB7633.
[35] Brou Boni KND, Klein J, Gulyban A, Reynaert N, Pasquier D. Improving generalization in MR-to-CT synthesis in radiotherapy by using an augmented cycle generative adversarial network with unpaired data. Med Phys 2021;48:3003–10. https://doi.org/10.1002/MP.14866.